Evaluation of Colour Models for Computer Vision Using Cluster Validation Techniques

David Budden, Shannon Fenn, Alexandre Mendes, and Stephan Chalup

School of Electrical Engineering and Computer Science
Faculty of Engineering and Built Environment
The University of Newcastle, Callaghan, NSW, 2308, Australia
{david.budden,shannon.fenn}@uon.edu.au,
{alexandre.mendes,stephan.chalup}@newcastle.edu.au

Abstract. Computer vision systems frequently employ colour segmentation as a step of feature extraction. This is particularly crucial in an environment where important features are colour-coded, such as robot soccer. This paper describes a method for determining an appropriate colour model by measuring the compactness and separation of clusters produced by the k-means algorithm. *RGB*, *HSV*, YC_bC_r and *CIE* $L^*a^*b^*$ colour models are assessed for a selection of artificial and real images, utilising an implementation of the Dunn's-based cluster validation index. The effectiveness of the method is assessed by qualitatively comparing the relative correctness of the segmentation to the results of the cluster validation. Results demonstrate a significant variation in segmentation quality among colour spaces, and that $\mathrm{YC}_b\mathrm{C}_r$ is the best choice for the DARwIn-OP platform tested.

Keywords: Image segmentation, colour representations, colour space analysis, clustering, cluster validation, pattern recognition.

1 Introduction

In computer vision, a mapping from an arbitrary 3-component colour space C to a set of colours M assigns a class label $m_i \in M$ to every point $c_j \in C$ [18]. If each channel is represented by an n-bit value and $k = |M|$ represents the number of defined class labels, then

$$C \to M, \tag{1}$$

where

$$C = \{0, 1, \ldots, 2^n - 1\}^3 \quad \text{and} \quad M = \{m_0, m_1, \ldots, m_{k-1}\}. \tag{2}$$

Concretely, in a colour space C, each pixel in an image is represented by a triplet with each value representing the contribution of each component to the overall colour of that pixel. Projecting the pixel values into the colour space constructed by the orthogonal component axes results in a projected colour space distribution of the original image. Points within the projected distribution

X. Chen et al. (Eds.): RoboCup 2012, LNAI 7500, pp. 261–272, 2013.

are typically clustered about centroids, which represent the predominant colours within the image. Therefore, in an image where the colour clusters are compact and well separated, a clustering algorithm such as k-means [7, 12, 20] is able to automate the process of colour segmentation. This is particularly applicable in an environment where important features are uniquely coloured, such as robot soccer [15]. Where computational resources are limited, the colour segmentation process is performed off-line, with the resultant mapping represented in the form of a $2^n \times 2^n \times 2^n$ look-up table (LUT). This LUT can then be used for efficient, real-time colour classification.

Many techniques exist for effective colour segmentation, including mean-shift and mode finding clustering [4, 7, 16, 19, 20]. Unfortunately, there are no general algorithms or colour models that are suited to all colour images [3]. Instead, this paper compares four common colour models: *RGB* [2, 3, 7, 20]; *HSV* [2, 3, 7, 13, 19, 20], YC_bC_r [3, 13, 20] and *CIE L*a*b** [3, 7, 20]) and proposes a method to assess their suitability for unsupervised colour segmentation by measuring the compactness and separation of clusters produced by the k-means algorithm. Robot soccer is chosen as a suitable colour-coded environment for testing the procedure [15], but it is anticipated that the procedure could be extended to determine the optimal colour model in other equivalent scenarios.

This paper is organised as follows: Sect. 2 describes the colour models tested; Sect. 3 describes the performance metrics used to validate the clusters obtained; Sect. 4 describes the test images; Sect. 5 presents the computational results; and finally, Sect. 6 and Sect. 7 provide a discussion and qualitative assessment of the results, followed by the conclusion.

2 Colour Models

2.1 RGB

The RGB colour model is a space in which each colour is represented by a combination of tristimuli R (red), G (green) and B (blue) [3]. Any colour can be created by exactly one combination of these three colour bases, which are defined according to their wavelength (700.0 nm for red, 546.1 nm for green and 435.8 nm for blue [20]). Although it is intuitive to represent colour in such a manner, RGB suffers from sensitivity to variations in illumination due to the high correlation of its three components [2–4, 19].

2.2 HSV

The HSV colour model separates information regarding the chrominance and intensity values of a colour by projecting the RGB colour space onto a non-linear chroma value H (hue), a radial saturation percentage S (saturation) and a luminance-inspired value V (value) [3, 7, 20]. The HSV colour model is frequently used for colour segmentation as the individual colour components are independent of the image brightness [3, 16, 19], resulting in more uniform clusters

for similar chrominance values [16]. Among the disadvantages, the H component is an angular value and therefore wraps around from 2π to zero, potentially resulting in the splitting of clusters to opposite ends of the hue axis. Furthermore, the nonlinear transformation results in high susceptibility to noise for low values of V [3].

2.3 $\mathrm{YC}_b\mathrm{C}_r$

Similarly to HSV, $\mathrm{YC}_b\mathrm{C}_r$ separates chrominance information into two channels C_b (blue chroma) and C_r (red chroma), and intensity into a third channel Y (luma) [3, 20]. The $\mathrm{YC}_b\mathrm{C}_r$ colour space can be obtained applying the following linear transformation to the RGB space:

$$\begin{bmatrix} Y' \\ C_b \\ C_r \end{bmatrix} = \begin{bmatrix} 0.299 & 0.587 & 0.114 \\ -0.168736 & -0.331264 & 0.5 \\ 0.5 & -0.418688 & -0.081312 \end{bmatrix} \begin{bmatrix} R' \\ G' \\ B' \end{bmatrix} + \begin{bmatrix} 0 \\ 128 \\ 128 \end{bmatrix}, \tag{3}$$

where R', G' and B' are 8-bit gamma-compressed colour components [20]. Although much of the component correlation found in RGB is removed, it still exists in part due to the linear nature of the transformation [3].

2.4 CIE L*a*b*

The CIE (Commission International de l'Eclairage) XYZ colour system, similarly to RGB, defines three tristimulis X, Y and Z, which can be combined to create any colour. Any colour can be created by linear combination of positive quantities of each component [3, 7, 20] (unlike RGB, which requires a negative amount of red light to be added to obtain certain colours in the blue-green range [20]). The CIE XYZ colour space can be obtained by applying the following linear transformation to the RGB space [20]:

$$\begin{bmatrix} X \\ Y \\ Z \end{bmatrix} = \frac{1}{0.17697} \begin{bmatrix} 0.49 & 0.31 & 0.20 \\ 0.17697 & 0.81240 & 0.01063 \\ 0.00 & 0.01 & 0.99 \end{bmatrix} \begin{bmatrix} R \\ G \\ B \end{bmatrix}. \tag{4}$$

The CIE L*a*b* (CIELAB) colour space applies nonlinear transformations to CIE XYZ to more accurately reflect the logarithmic manner in how humans perceive differences in chromaticity and luminance [3, 7, 20]. For a nominal white value (X_n, Y_n, Z_n) (chosen as the CIE D65 standard $(0.9642, 1, 0.8249)$), the L^* (lightness) component is defined as [20]

$$L^* = 116 f\left(\frac{Y}{Y_n}\right), \quad f(t) = \begin{cases} t^{1/3} & \text{, if } t > \delta^3 \\ t/(3\delta^2) + 2\delta/3 & \text{, otherwise} \end{cases} \tag{5}$$

where $\delta = 6/29$, resulting in a value in the range $[0, 100]$. Similarly, a^* and b^* are defined as [20]

$$a^* = 500\left[f\left(\frac{X}{X_n}\right) - f\left(\frac{Y}{Y_n}\right)\right] \quad \text{and} \quad b^* = 200\left[f\left(\frac{Y}{Y_n}\right) - f\left(\frac{Z}{Z_n}\right)\right]. \tag{6}$$

2.5 Linear Transformation Orthogonality

As the transformations from RGB to HSV and CIELAB are nonlinear, it is intuitive that k-means clustering within each of these spaces will yield different results for a given image. This is not inherently the case for the linear transformation from RGB to $\mathrm{YC}_b\mathrm{C}_r$, therefore it should be demonstrated that the transformation is not orthogonal (does not preserve Euclidean distance). Given a linear transformation M, it is known from linear algebra that

$$\sigma_{min}\|v\| \leq \|Mv\| \leq \sigma_{max}\|v\|, \tag{7}$$

where σ_{min} and σ_{max} are the minimum and maximum *singular values* resulting from the singular value decomposition of M [8]. For (3), these values are equal to 0.4589 and 0.8039 respectively, resulting in a condition number of $\sigma_{max}/\sigma_{min} = 1.7518 \neq 1$. Therefore it can be said with confidence that k-means will yield clusters of varying quality for every colour space described in Sect. 2.

3 Performance Metrics

The performance of a clustering algorithm within a given feature space is reflected in the quality of the resulting clusters in that space. The process of evaluating the quality of a cluster is referred to as *cluster validation*, of which three main categories exist [11]:

- *External Criteria:* Involves evaluating the clustering results based on human-defined "expected results", such as correctly identified colours within an image.
- *Internal Criteria:* Involves evaluating the clustering results in terms of the input data itself, by measuring values such as *compactness* (density of a cluster, also known as *intracluster similarity*) and *separation* (distance between clusters, also known as *intercluster dissimilarity*).
- *Relative Criteria:* Involves evaluating the clustering results in terms of its similarity to other results produced by the same algorithm, but with different parameter values.

This paper deals primarily with the application of internal criteria to produce quantitative results (see Sect. 5), with a discussion of external criteria provided in Sect. 6. Many internal criteria performance metrics have been suggested for assessing the validity of cluster partitions [9], including the *Silhouette method* [1, 17], *Dunn's based index* [1, 6, 9], *Davies-Bouldin index* [1, 5, 9] and *C-index* [1, 9, 14]. In this paper, the Dunn's index was chosen as most suitable for validating cluster partitions within the colour spaces described in Sect. 1, as it has low computational complexity and does not rely on presumptions regarding the shape or relative sizes of clusters [9].

3.1 Dunn's Index

For any partition $X = X_1 \cup \ldots X_i \cup \ldots X_k$, with k clusters, where X_i represents the i^{th} cluster of such a partition, the Dunn's index, D, is defined as [1, 6, 9]

$$D(X) = \min_{1 \leq i \leq k} \left\{ \min_{\substack{1 \leq j \leq k \\ j \neq i}} \left\{ \frac{\delta(X_i, X_j)}{\max_{1 \leq l \leq k} \{\Delta(X_l)\}} \right\} \right\}, \tag{8}$$

where $\delta(X_i, X_j)$ is the intercluster distance between clusters i and j; and $\Delta(X_l)$ is the intracluster distance for cluster l. The aim of this metric is maximise $D(X)$, by maximising the minimum intercluster distance $\delta(X_i, X_j)$, whilst minimising the maximum intracluster distance. As Dunn's index is calculated using only two distances it is particularly susceptible to outliers [9], therefore is is important that the distance functions $\delta(X_i, X_j)$ and $\Delta(X_l)$ be chosen in such a way as to minimise the impact of chromatic noise.

3.2 Methods of Calculating Distances

Among the possible distance metrics, *Euclidean distance* was chosen to determine the distance between two sample points, as required for the intercluster and intracluster distance calculations (discussed below). Euclidean distance was chosen for consistency with the k-means implementation utilised.

Intercluster Distances: Several methods have been suggested for calculating the intercluster distance between clusters X_i and X_j [1, 11], including:

- *Single linkage*: Shortest distance between any two objects, each belonging to separate clusters X_i and X_j.
- *Complete linkage*: Greatest distance between any two objects, each belonging to separate clusters X_i and X_j.
- *Average linkage*: Average distance between all pairs of points belonging to separate clusters X_i and X_j.
- *Centroid linkage*: Distance between the centroids of clusters X_i and X_j.
- *Average to centroids*: Average distance between the centroid of cluster X_i and all the points belonging to cluster X_j.

Of these, the average to centroids linkage was chosen as a good trade-off between outlier sensitivity and computational complexity. For two clusters X_i and X_j belonging to partition X, the average to centroids linkage $\delta(X_i, X_j)$ is defined as

$$\delta(X_i, X_j) = \frac{1}{|X_i| + |X_j|} \left(\sum_{x \in X_i} d(x, C_{X_j}) + \sum_{y \in X_j} d(y, C_{X_i}) \right), \tag{9}$$

where the cluster centroids C_{X_i} and C_{X_j} are defined as

$$C_{X_i} = \frac{1}{|X_i|} \sum_{x \in X_i} x \qquad C_{X_j} = \frac{1}{|X_j|} \sum_{y \in X_j} y. \tag{10}$$

Intracluster Distances: As with the intercluster distances, there exists several methods of calculating the intracluster distance of a cluster X_i, including [1]:

- *Complete diameter*: Greatest distance between any two points belonging to the cluster.
- *Average diameter*: Average distance between all pairs of points belonging to the cluster.
- *Centroid diameter*: Average distance between the cluster centroid and all points belonging to that cluster.

Of these, centroid diameter was chosen, again as a good trade-off between sensitivity and complexity. For a cluster X_i belonging to partition X, the centroid diameter $\Delta(X_i)$ is defined as

$$\Delta(X_i) = 2\left(\frac{\sum_{x \in X_i} d(x, C_{X_i})}{|X_i|}\right), \tag{11}$$

where the cluster centroid C_{X_i} is defined as in (10).

4 Test Images

This paper utilises a series of images[1], some artificially generated and some captured using the DARwIn-OP's 2MP camera [10]. Robot soccer [15] was chosen as an example of a colour-coded environment, where important features to be identified are assigned different colours. As not all features will be present in every vision frame, two images were selected to represent common soccer scenarios. The first image (see Table 1, bottom-right corner) has the camera pointed towards the ground, and contains only the field, field lines and the ball. Therefore, only three main colours are present. The second image (see Table 2, bottom-right corner) demonstrates the camera pointed toward the goal, adding a robot and goalposts to the image and therefore increasing the number of main colours to five.

To understand how the system reacts to the presence of noise in an "ideal" image, a set of artificial data was generated for each image. They consist of homogeneous blocks of colours representative of those of the image features at varying levels of Gaussian noise (10%, 20% and 30%, see Tables 1 and 2). As the feature spaces for clustering are exactly the colour spaces described in Sect. 2, the results are independent of pixel position, therefore the Gaussian noise should have an effect similar to the introduction of a variety of coloured, unimportant objects into actual vision frames. Common examples of such "noise" include a cable extended over the field or a spectator watching the match.

5 Experimental Results

The experimental results are illustrated by two groups of images, containing three and five colours respectively. k-means clustering was applied to all test

[1] Available at: `http://www.davidbudden.com/research/colour-model-evaluation/`

images described in Sect. 4 in each colour space described in Sect. 2. The range for the number of clusters for each image was chosen to be no less than the number of features identifiable in the images, therefore the values of k tested were chosen as $k = \{3, 4, \ldots, 10\}$ for the images in Table 1, and $k = \{5, 6, \ldots, 12\}$ for those in Table 2.

The Dunn's index was applied as a method of evaluating the performance of the clustering in each colour space by calculating the compactness and separation of resultant clusters, as described in Sect. 3. The process of clustering and validation for each image, colour space and k value was repeated 100 times to allow for variations in performance due to the random initial placement of the cluster centroids in the k-means algorithm. Tables 1 and 2 demonstrate the mean values over those 100 runs, with the optimal values indicated in bold.

Table 1 demonstrates that for a small number of predominant colours and a low level of chromatic noise, clusters within the RGB colour space are overall more compact and separated. Additional chromatic noise resulted in better clustering within the YC_bC_r colour space and for a larger k value, equal to four. It should also be noted that the standard deviation values were quite low, implying that either all 100 k-means runs converged to the same local minimum, or to several local minima with similar Dunn's index values.

Table 2 shows the results for a larger number of predominant colours. YC_bC_r outperforms RGB, HSV and CIELAB colour spaces in all images, irrespective of noise level. RGB also performs quite well. The standard deviation values are considerably higher than for three predominant colours; in particular, the standard deviation for YC_bC_r (k=5) is very high. After a thorough analysis of a repeated trial, four local optima with observed, with Dunn's index values of 0.32 (obtained 29 times), 0.31 (35 times), 0.09 (10 times) and 0.04 (26 times). Despite YC_bC_r appearing to be the best colour space, further tests with a larger number of real images should be conducted in the future to determine the reliability of this outcome.

Analysing Tables 1 and 2 as a whole, it can be concluded that RGB and YC_bC_r demonstrate consistently better results than HSV and CIELAB, irrespective of the the image tested. A qualitative assessment of these results is presented in Section 6.

6 Discussion

The results in Sect. 5 demonstrate that for images with either more than three predominant features or greater than 20% chromatic noise, k-means produced clusters with maximum compactness and separation when performed in the YC_bC_r colour space. However, for this to be an accurate measure of the colour segmentation performance, it is crucial that the clusters correspond with the actual set of feature colours. In order to verify how representative the clusters found by the k-means are of the real colours in the image, a series of images are presented in Fig. 1. As an example, the image in Table 2 contains five uniquely coloured features - the green field, white lines, black robot, yellow goalposts and

Table 1. Cluster quality evaluation using the Dunn's index for the images with three dominant colours. The four colour spaces were tested using four images: three artificially created, with Gaussian noise levels of 10%, 20% and 30%; and one original image, captured with the DARwIn-OP camera [10]. The figures represent the mean of 100 runs of the k-means algorithm; the standard deviation is indicated in parentheses. The RGB colour space demonstrated better performance for low noise levels, whereas YC_bC_r performed better for higher noise levels and the original image.

3 colours - 10% noise

Colour space	Number of clusters (k)								
	3	**4**	**5**	**6**	**7**	**8**	**9**	**10**
RGB	**3.66** (0.00)	0.50 (0.00)	0.23 (0.11)	0.16 (0.11)	0.11 (0.08)	0.10 (0.06)	0.09 (0.02)	0.08 (0.03)
HSV	0.15 (0.00)	0.38 (0.06)	0.12 (0.03)	0.21 (0.01)	0.50 (0.04)	0.24 (0.02)	0.23 (0.04)	0.15 (0.08)
YC_bC_r	3.00 (0.00)	0.56 (0.00)	0.39 (0.26)	0.40 (0.10)	0.28 (0.06)	0.20 (0.10)	0.16 (0.11)	0.11 (0.09)
CIELAB	1.11 (0.00)	0.25 (0.00)	0.18 (0.03)	0.21 (0.00)	0.23 (0.03)	0.29 (0.06)	0.22 (0.09)	0.19 (0.04)

3 colours - 10% noise

3 colours - 20% noise

Colour space	Number of clusters (k)								
	3	**4**	**5**	**6**	**7**	**8**	**9**	**10**
RGB	**1.01** (0.00)	0.59 (0.00)	0.30 (0.01)	0.32 (0.02)	0.34 (0.09)	0.32 (0.09)	0.30 (0.04)	0.29 (0.01)
HSV	0.34 (0.00)	0.17 (0.01)	0.31 (0.08)	0.22 (0.03)	0.22 (0.00)	0.23 (0.00)	0.18 (0.06)	0.11 (0.02)
YC_bC_r	0.83 (0.00)	0.72 (0.00)	0.35 (0.00)	0.55 (0.00)	0.34 (0.02)	0.34 (0.07)	0.34 (0.05)	0.32 (0.03)
CIELAB	0.32 (0.00)	0.35 (0.00)	0.19 (0.00)	0.23 (0.00)	0.29 (0.00)	0.32 (0.02)	0.19 (0.02)	0.15 (0.00)

3 colours - 20% noise

3 colours - 30% noise

Colour space	Number of clusters (k)								
	3	**4**	**5**	**6**	**7**	**8**	**9**	**10**
RGB	0.52 (0.00)	0.58 (0.00)	0.32 (0.00)	0.45 (0.00)	0.40 (0.05)	0.38 (0.02)	0.37 (0.02)	0.35 (0.02)
HSV	0.33 (0.00)	0.38 (0.00)	0.18 (0.01)	0.20 (0.01)	0.21 (0.01)	0.13 (0.01)	0.14 (0.03)	0.16 (0.03)
YC_bC_r	0.47 (0.00)	**0.75** (**0.00**)	0.42 (0.00)	0.53 (0.00)	0.30 (0.01)	0.32 (0.02)	0.35 (0.02)	0.41 (0.03)
CIELAB	0.26 (0.00)	0.23 (0.01)	0.24 (0.00)	0.18 (0.00)	0.18 (0.01)	0.17 (0.01)	0.19 (0.00)	0.16 (0.03)

3 colours - 30% noise

3 colours - Original image

Colour space	Number of clusters (k)								
	3	**4**	**5**	**6**	**7**	**8**	**9**	**10**
RGB	0.11 (0.00)	0.11 (0.01)	0.09 (0.00)	0.04 (0.00)	0.05 (0.01)	0.05 (0.01)	0.05 (0.01)	0.04 (0.01)
HSV	0.11 (0.00)	0.08 (0.00)	0.06 (0.00)	0.04 (0.00)	0.04 (0.00)	0.05 (0.01)	0.05 (0.00)	0.05 (0.01)
YC_bC_r	0.11 (0.00)	**0.12** (**0.00**)	0.12 (0.01)	0.05 (0.01)	0.05 (0.01)	0.05 (0.01)	0.04 (0.01)	0.04 (0.01)
CIELAB	0.10 (0.00)	0.11 (0.00)	0.07 (0.00)	0.07 (0.02)	0.07 (0.02)	0.04 (0.01)	0.04 (0.01)	0.03 (0.00)

3 colours - Original

Table 2. Cluster quality evaluation using the Dunn's index for images with five dominant colours. The YC_bC_r colour space demonstrated the best performance, irrespective of the noise level. In addition, the optimal Dunn's index value was obtained with $k = 5$ on all four images. It should be noted that RGB also maintained a good overall performance.

5 colours - 10% noise

Colour space	Number of clusters (k)							
	5	**6**	**7**	**8**	**9**	**10**	**11**	**12**
RGB	1.86 (0.00)	0.53 (0.00)	0.74 (0.24)	0.32 (0.10)	0.29 (0.07)	0.27 (0.06)	0.26 (0.05)	0.26 (0.03)
HSV	0.21 (0.00)	0.21 (0.01)	0.45 (0.08)	0.13 (0.02)	0.20 (0.06)	0.17 (0.08)	0.10 (0.06)	0.06 (0.02)
$\mathbf{YC_bC_r}$	**2.23 (0.00)**	0.60 (0.00)	1.07 (0.25)	0.48 (0.15)	0.33 (0.08)	0.29 (0.05)	0.29 (0.05)	0.27 (0.05)
CIELAB	0.24 (0.03)	0.33 (0.02)	0.26 (0.16)	0.17 (0.06)	0.18 (0.04)	0.19 (0.03)	0.18 (0.04)	0.19 (0.05)

5 colours - 10% noise

5 colours - 20% noise

Colour space	Number of clusters (k)							
	5	**6**	**7**	**8**	**9**	**10**	**11**	**12**
RGB	0.96 (0.00)	0.53 (0.01)	0.33 (0.03)	0.33 (0.02)	0.33 (0.07)	0.30 (0.05)	0.29 (0.04)	0.28 (0.03)
HSV	0.28 (0.04)	0.24 (0.02)	0.19 (0.00)	0.23 (0.03)	0.22 (0.03)	0.22 (0.03)	0.16 (0.05)	0.13 (0.04)
$\mathbf{YC_bC_r}$	**1.22 (0.00)**	0.63 (0.00)	0.43 (0.14)	0.50 (0.07)	0.33 (0.01)	0.37 (0.02)	0.38 (0.04)	0.33 (0.06)
CIELAB	0.20 (0.00)	0.26 (0.00)	0.24 (0.10)	0.21 (0.05)	0.22 (0.05)	0.27 (0.00)	0.27 (0.02)	0.30 (0.01)

5 colours - 20% noise

5 colours - 30% noise

Colour space	Number of clusters (k)							
	5	**6**	**7**	**8**	**9**	**10**	**11**	**12**
RGB	0.97 (0.00)	0.47 (0.07)	0.44 (0.03)	0.41 (0.04)	0.40 (0.04)	0.38 (0.06)	0.37 (0.05)	0.36 (0.05)
HSV	0.30 (0.00)	0.24 (0.02)	0.26 (0.03)	0.38 (0.10)	0.32 (0.04)	0.22 (0.01)	0.21 (0.01)	0.20 (0.01)
$\mathbf{YC_bC_r}$	**0.99 (0.00)**	0.67 (0.00)	0.84 (0.08)	0.43 (0.08)	0.42 (0.05)	0.41 (0.04)	0.40 (0.04)	0.40 (0.04)
CIELAB	0.34 (0.00)	0.29 (0.04)	0.32 (0.00)	0.33 (0.00)	0.31 (0.02)	0.38 (0.04)	0.44 (0.02)	0.36 (0.03)

5 colours - 30% noise

5 colours - Original image

Colour space	Number of clusters (k)							
	5	**6**	**7**	**8**	**9**	**10**	**11**	**12**
RGB	0.22 (0.04)	0.10 (0.04)	0.07 (0.02)	0.06 (0.01)	0.06 (0.01)	0.07 (0.02)	0.07 (0.03)	0.07 (0.03)
HSV	0.19 (0.00)	0.12 (0.01)	0.12 (0.01)	0.13 (0.04)	0.07 (0.02)	0.06 (0.02)	0.06 (0.03)	0.05 (0.03)
$\mathbf{YC_bC_r}$	**0.25 (0.12)**	0.06 (0.00)	0.06 (0.01)	0.06 (0.02)	0.07 (0.02)	0.07 (0.03)	0.08 (0.03)	0.07 (0.03)
CIELAB	0.07 (0.02)	0.06 (0.02)	0.05 (0.01)	0.05 (0.01)	0.05 (0.02)	0.05 (0.01)	0.05 (0.02)	0.06 (0.03)

5 colours - Original

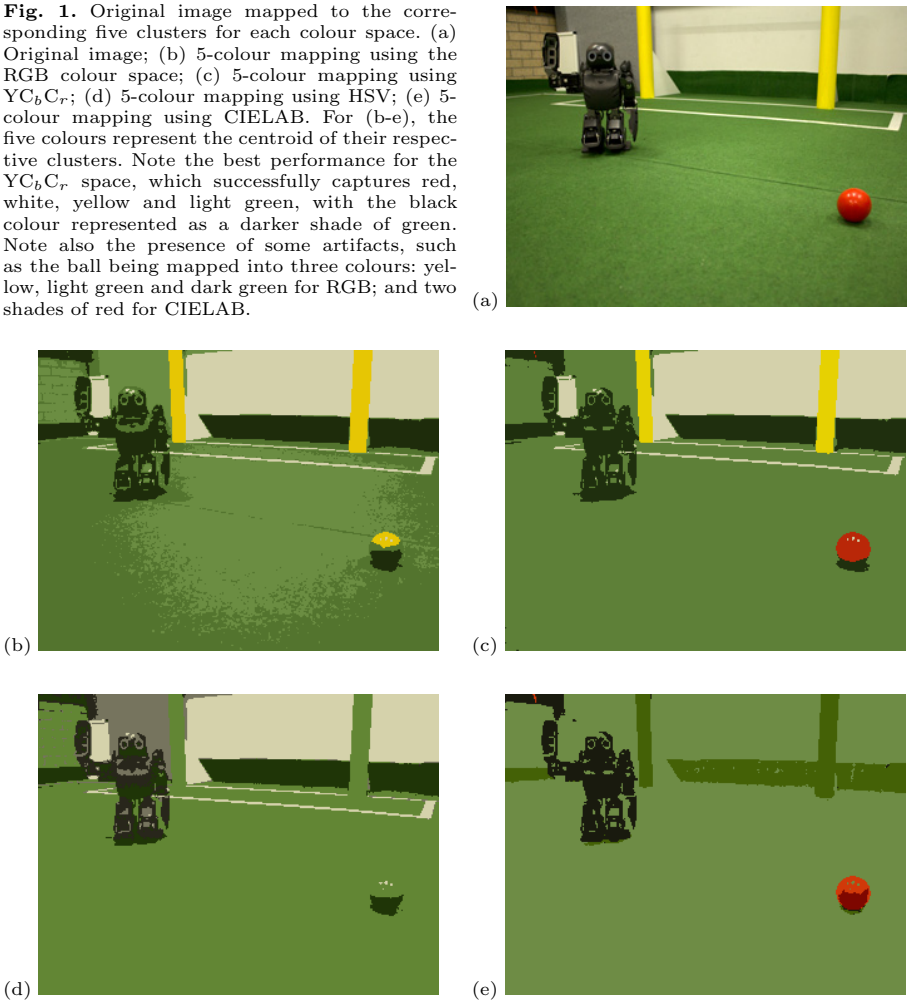

Fig. 1. Original image mapped to the corresponding five clusters for each colour space. (a) Original image; (b) 5-colour mapping using the RGB colour space; (c) 5-colour mapping using YC_bC_r; (d) 5-colour mapping using HSV; (e) 5-colour mapping using CIELAB. For (b-e), the five colours represent the centroid of their respective clusters. Note the best performance for the YC_bC_r space, which successfully captures red, white, yellow and light green, with the black colour represented as a darker shade of green. Note also the presence of some artifacts, such as the ball being mapped into three colours: yellow, light green and dark green for RGB; and two shades of red for CIELAB.

red ball. A correct segmentation should therefore map the pixels comprising each of these features to a unique colour label.

The pixels in the images in Fig. 1b-e were painted with the centroid values of the clusters that they were assigned to. However, given that 100 runs of the k-means algorithm were executed for each configuration of image and colour space, it is vital to determine with set of centroids was most representative of the overall results. After analysing the results for a given configuration, it was determined that the number of different solutions was never greater than five - i.e. the same sets of centroids were reached several times in those 100 runs. With that in mind, the centroid values used in each configuration depicted in Fig. 1b-e are the solutions that occurred most frequently.

Table 2 suggests the YC_bC_r colour space allows better clustering performance than the other three colour spaces for Fig. 1a. That assertion is confirmed by qualitatively assessing the result of applying k-means determine the main colours in the image (for $k = 5$). Fig. 1b shows that clustering in RGB failed to correctly label the red ball, which contains pixels that belong to three different clusters (yellow and two shades of green). In addition, it associated the field and the robot with three separate clusters, at different levels of green. In contrast, clustering in YC_bC_r (Fig. 1c) labeled each feature correctly. Figure 1d depicts the result for HSV; it fails to identify the goal post, assigning to it the same colour of the field. In addition, the ball contains two shades of green. Finally, Figure 1e depicts the result for CIELAB. It identifies the ball and the robot, but fails to identify the ball or field lines. This agreement between external and internal cluster validation criteria supports cluster validation as an effective method for assessing the appropriateness of a colour model for segmentation.

7 Conclusion

This work analysed the use of different colour spaces in the quality of colour classification in a computer vision system. The application of a Dunn's index cluster validation technique demonstrated that the k-means algorithm produced clusters of maximum compactness and separation in the YC_bC_r colour space, for images with five uniquely coloured features. RGB, HSV and CIELAB yielded poorer results independent of the level of chromatic noise present. For images with three uniquely coloured features, YC_bC_r yielded the best results for higher levels of chromatic noise, whereas RGB had a better performance for low levels of noise.

The quantitative results were also qualitatively assessed by visualising the colour segmentation for each colour model. In that case, the qualitative analysis of the YC_bC_r results confirmed the numerical results. Correct segmentation corresponded with higher values of the Dunn's-based index, therefore supporting cluster validation as an effective technique of assessing the performance of a colour model for segmentation within a colour-coded environment.

Future research will focus on automating the LUT generation process for DARwIn-OP platform, allowing for efficient real-time colour image segmentation whilst minimising the requirement for human supervision.

Acknowledgement. David Budden and Shannon Fenn would like to thank the University of Newcastle's Faculty of Engineering and Built Environment for the support provided by their Summer Research Scholarship program.

References

1. Bolshakova, N., Azuaje, F.: Cluster validation techniques for genome expression data. Signal Processing 83(4), 825–833 (2003)
2. Brusey, J., Padgham, L.: Techniques for obtaining robust, real-time, colour-based vision for robotics. In: Veloso, M.M., Pagello, E., Kitano, H. (eds.) RoboCup 1999. LNCS (LNAI), vol. 1856, pp. 243–253. Springer, Heidelberg (2000)

3. Cheng, H., Jiang, X., Sun, Y., Wang, J.: Color image segmentation: advances and prospects. Pattern Recognition 34(12), 2259–2281 (2001)
4. Comaniciu, D., Meer, P.: Mean shift: A robust approach toward feature space analysis. IEEE Transactions on Pattern Analysis and Machine Intelligence 24(5), 603–619 (2002)
5. Davies, D., Bouldin, D.: A cluster separation measure. IEEE Transactions on Pattern Analysis and Machine Intelligence (2), 224–227 (1979)
6. Dunn, J.: Well-separated clusters and optimal fuzzy partitions. Journal of Cybernetics 4(1), 95–104 (1974)
7. Forsyth, D., Ponce, J.: Computer vision: a modern approach. Prentice Hall (2002)
8. Golub, G., Van Loan, C.: Matrix computations, vol. 3. Johns Hopkins University Press (1996)
9. Günter, S., Bunke, H.: Validation indices for graph clustering. Pattern Recognition Letters 24(8), 1107–1113 (2003)
10. Ha, I., Tamura, Y., Asama, H., Han, J., Hong, D.: Development of open humanoid platform DARwIn-OP. In: 2011 Proceedings of the SICE Annual Conference (SICE), pp. 2178–2181. IEEE (2011)
11. Halkidi, M., Batistakis, Y., Vazirgiannis, M.: On clustering validation techniques. Journal of Intelligent Information Systems 17(2), 107–145 (2001)
12. Hartigan, J., Wong, M.: Algorithm AS 136: A k-means clustering algorithm. Journal of the Royal Statistical Society. Series C (Applied Statistics) 28(1), 100–108 (1979)
13. Henderson, N., King, R., Chalup, S.: An automated colour calibration system using multivariate gaussian mixtures to segment HSI colour space. In: Proceedings of the 2008 Australasian Conference on Robotics & Automation (ACRA 2008) (2008)
14. Hubert, L., Schultz, J.: Quadratic assignment as a general data analysis strategy. British Journal of Mathematical and Statistical Psychology 29(2), 190–241 (1976)
15. Kitano, H., Asada, M., Kuniyoshi, Y., Noda, I., Osawa, E.: Robocup: The robot world cup initiative. In: Proceedings of the First International Conference on Autonomous Agents, pp. 340–347. ACM (1997)
16. Park, J., Lee, G., Park, S.: Color image segmentation using adaptive mean shift and statistical model-based methods. Computers & Mathematics with Applications 57(6), 970–980 (2009)
17. Rousseeuw, P.: Silhouettes: a graphical aid to the interpretation and validation of cluster analysis. Journal of Computational and Applied Mathematics 20, 53–65 (1987)
18. Sridharan, M., Stone, P.: Real-time vision on a mobile robot platform. In: 2005 IEEE/RSJ International Conference on Intelligent Robots and Systems (IROS 2005), pp. 2148–2153. IEEE (2005)
19. Sural, S., Qian, G., Pramanik, S.: Segmentation and histogram generation using the HSV color space for image retrieval. In: Proceedings of the 2002 International Conference on Image Processing, vol. 2, pp. II–589. IEEE (2002)
20. Szeliski, R.: Computer vision: algorithms and applications. Springer-Verlag New York Inc. (2010)